

Theoretical Models of Photodissociation Fronts

By **B. T. Draine**¹
AND **Frank Bertoldi**²

¹Princeton University Observatory, Princeton, NJ 08544-1001, USA

²Max-Planck-Institut für Radioastronomie, D-53121 Bonn, Germany

Observations of H₂ line emission have revealed higher-than-expected gas temperatures in a number of photodissociation fronts. We discuss the heating and cooling processes in photodissociation regions. Observations of NGC 2023 are compared to a theoretical model in which there is substantial gas at temperatures $T = 500 - 1000\text{K}$ heated by photoelectric emission and collisional deexcitation of H₂. In general the model successfully reproduces the observed H₂ line emission from a wide range of energy levels. The observed [SiII]34.8 μm emission appears to indicate substantial depletion of Si in NGC 2023.

1. Introduction

A significant fraction of the ultraviolet radiation emitted by massive stars impinges on the molecular gas associated with star formation. The resulting photodissociation regions (PDRs) therefore play an important role in reprocessing the energy flow in star-forming galaxies. Modelling these PDRs is therefore an important theoretical challenge, both to test our understanding of the physical processes in interstellar gas, and to interpret observations of star-forming galaxies.

It is frequently the case that the illuminating star is hot enough to produce an H II region, in which case the photodissociation region is bounded on one side by an ionization front, and on the other by cold molecular gas which has not yet been appreciably affected by ultraviolet radiation. The $h\nu < 13.6\text{eV}$ photons propagating beyond the ionization front raise the fractional ionization, photoexcite and photodissociate the H₂, and heat the gas via photoemission from dust and collisional deexcitation of vibrationally-excited H₂. Figure 1 shows the different layers within a PDR.

2. PDR Thermometry

The lower rotational levels of H₂ tend to be in LTE (except perhaps for the ortho/para ratio, which adjusts relatively slowly), so we can use the relative level populations of H₂ as a PDR thermometer.

We can also use the absolute column densities $N(v, J)$ to tell us how much molecular gas is at different temperatures. Because the H₂ quadrupole vibration-rotation lines are generally optically thin, only dust extinction affects the radiative transfer.

The level populations $N(v, J)$ can be studied using vibrational transitions (ground-based K,H,J,I,R band spectroscopy) or $v=0-0$ pure rotation lines (some from the ground, but mainly from space, with ISO or SIRTf, or from the stratosphere, with SOFIA).

3. Modeling PDRs

The central physical process in a PDR is the photoexcitation and photodissociation of H₂ through the Lyman and Werner band lines of H₂, and it is therefore important

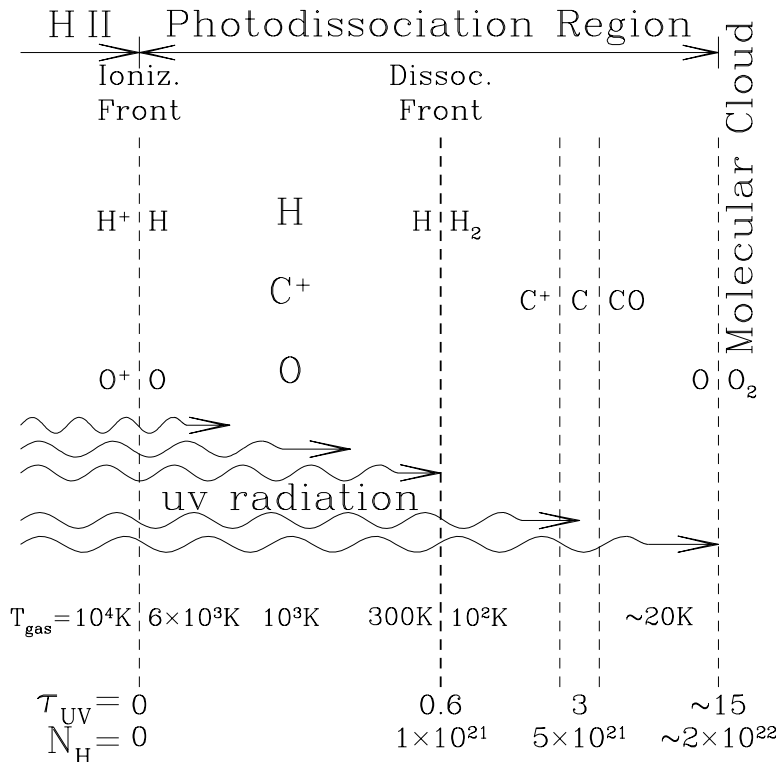


FIGURE 1. Schematic diagram showing the different zones in a photodissociation region.

to model this process accurately. In our models (Draine & Bertoldi 1996) we explicitly include radiative transfer in the 28765 permitted Lyman and Werner band lines between H_2 levels with $J \leq 29$, using wavelengths and oscillator strengths from Abgrall & Roueff (1989) and Abgrall et al. (1993a,b). The lines are treated independently assuming Voigt line profiles and attenuation by dust, but we include a statistical correction for the effects of line overlap of the H_2 lines (Draine & Bertoldi 1996).

Lyman and Werner band photons are absorbed by H_2 in the ground electronic state $X^1\Sigma_g^+$, resulting in excitation to vibration-rotation levels of either the $B^1\Sigma_u^+$ or $C^1\Pi_u^\pm$ electronic states. The electronically-excited state will decay by spontaneous emission of an ultraviolet photon. About 85% of the downward transitions will be to a bound (v, J) level of the ground electronic state, but about 15% of the transitions will be to the vibrational continuum of the ground electronic state, producing two H atoms, typically moving apart with a kinetic energy of a fraction of ~ 1 eV (Stephens & Dalgarno 1973).

Bertoldi & Draine (1996) discussed the propagation of coupled ionization-dissociation fronts, and showed that except when the PDR is driven by radiation from a very hot star, it is usually the case that the PDR moves into the molecular cloud slowly enough that thermal and chemical conditions are close to being in steady-state balance: most importantly, H_2 destruction is nearly balanced by H_2 formation, and heating is nearly balanced by cooling. It is then convenient to approximate the structure of the PDR by requiring precise thermochemical steady state at each point. The H_2 abundance is therefore determined by a balance between destruction by photodissociation and formation

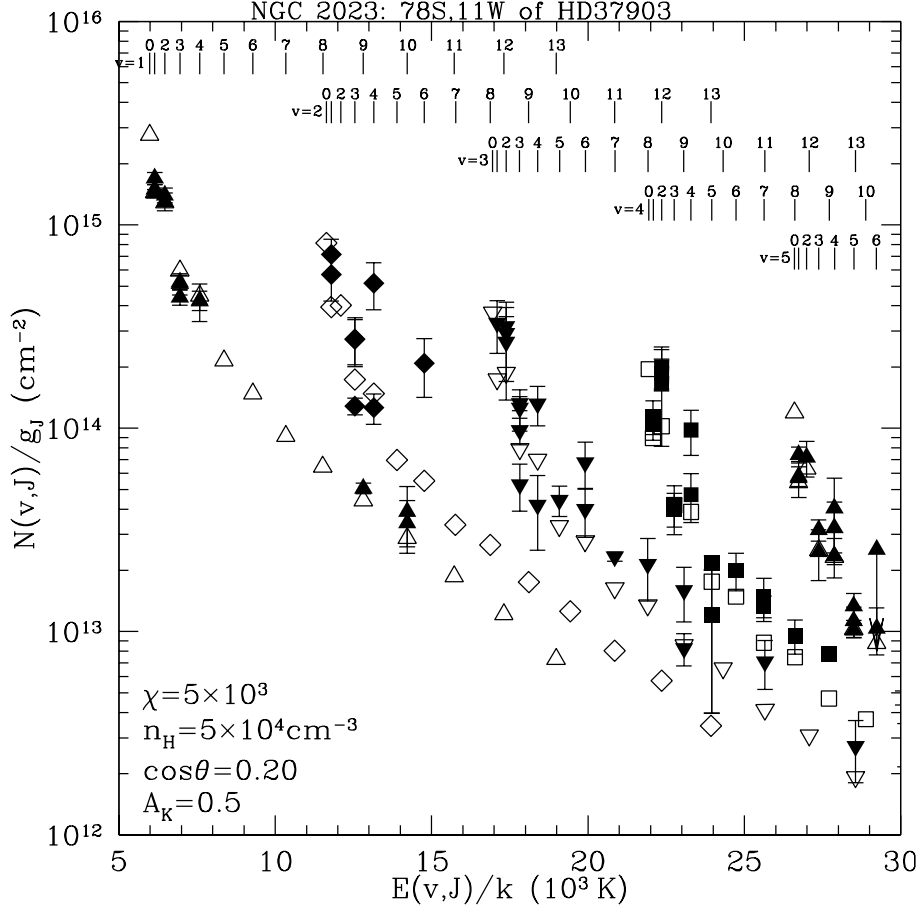


FIGURE 2. $N(v, J)/g_J$ for vibrationally-excited levels of H_2 toward the southern bar in NGC 2023. Open symbols: plane-parallel model with $n_{\text{H}} = 5 \times 10^4 \text{cm}^{-3}$ and $\chi = 5000$ observed from angle $\theta = 78^\circ$ rel. to surface normal. Filled symbols: level populations obtained from observed line intensities after correction for foreground extinction with $A_K = 0.5 \text{mag}$. Data from Burton et al. (1998) and McCartney et al. (1999).

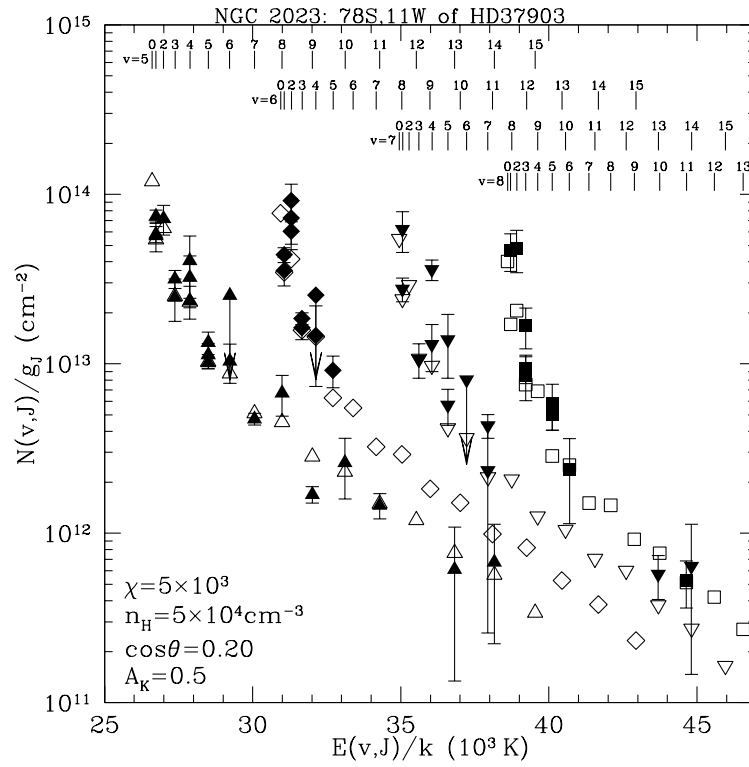
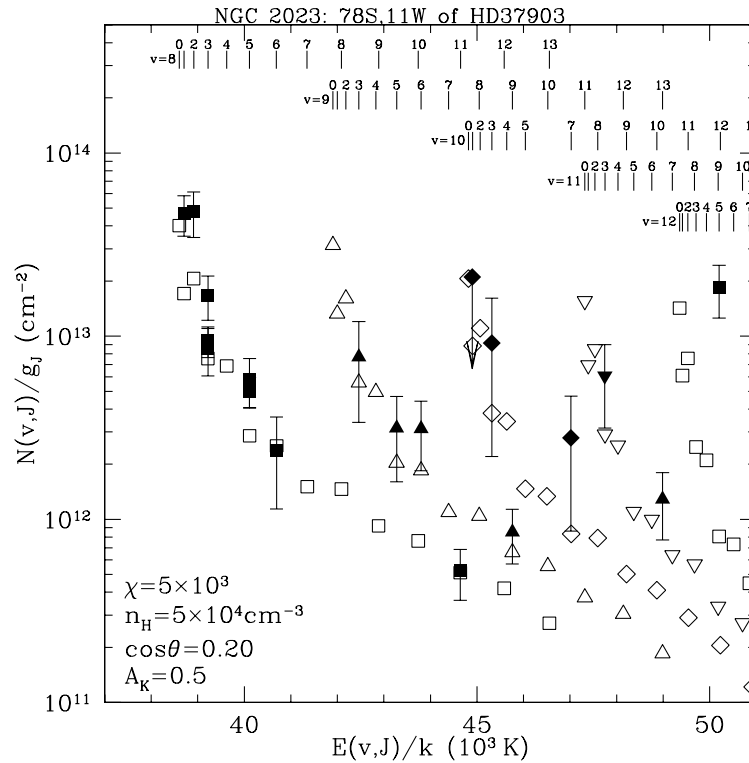
on grains,

$$R_{gr} n_{\text{H}} n(\text{H}) = \zeta_{pd} n(\text{H}_2) \quad (3.1)$$

where ζ_{pd} is the local rate for photodissociation of H_2 , and R_{gr} is the rate coefficient for H_2 formation on grains, with the grain abundance assumed proportional to $n_{\text{H}} \equiv 2n(\text{H}_2) + n(\text{H}) + n(\text{H}^+)$. We solve for the steady-state populations of the 299 bound (v, J) levels with $J \leq 29$, including UV pumping, spontaneous decay, and collisional transitions. The distribution over (v, J) of newly-formed H_2 produced on grain surfaces is uncertain; our models allow us to consider various possibilities.

The gas is heated primarily by photoelectrons ejected from dust grains, and (for densities $n_{\text{H}} \gtrsim 10^4 \text{cm}^{-3}$) collisional deexcitation of vibrationally-excited H_2 resulting from UV pumping. In our models we use photoelectric heating rates estimated by Weingartner & Draine (2000a); we assume dust with $R_V = 5.5$ with 5% of the solar carbon in ultrasmall carbonaceous grains.

The cooling of the gas is dominated by $[\text{CII}]158\mu\text{m}$, $[\text{SiII}]35\mu\text{m}$, $[\text{OI}]63\mu\text{m}$, and $[\text{FeII}]26\mu\text{m}$. The $[\text{OI}]63\mu\text{m}$ line is often optically thick; we use an escape probability treatment.

FIGURE 3. Same as Fig. 2, but for $v = 5 - 8$.FIGURE 4. Same as Fig. 2, but for $v = 8 - 12$.

4. NGC 2023: A Test Case

The B1.5V star HD 37903 is situated just outside the surface of the L1630 molecular cloud, resulting in the famous reflection nebula NGC 2023. Many emission lines of H_2 have now been measured for NGC 2023, making it an ideal test for PDR models. High resolution images of NGC 2023 in the 1-0S(1) line have recently been published (Rouan et al. 1997; Field et al. 1998; McCartney et al. 1999), showing pronounced filamentary structure, notably strong emission along the “southern bar” 78” south of HD 37903.

Black & van Dishoeck (1987) produced the first models to explain the H_2 fluorescence from NGC 2023. Their favored model assumed cold H_2 with a density $n_{\text{H}} \approx 10^4 \text{cm}^{-3}$ and an ultraviolet radiation field enhanced by a factor $\chi \approx 700$ relative to the Habing (1968) intensity. Draine & Bertoldi (1996) argued that some warm gas with $T \approx 500 - 1000\text{K}$ with density $n_{\text{H}} \approx 10^5 \text{cm}^{-3}$ was required to explain the observed line ratios.

New observations have become available both from the ground (Burton et al. 1998; McCartney et al. 1999) and from ISO (Bertoldi et al. 2000a). From ground-based spectrophotometry of the bright “southern emission bar” it is now clear that the foreground extinction at K is $A_K \approx 0.5\text{mag}$, implying a far-red extinction $A_{0.8\mu\text{m}} \approx 2.7\text{mag}$. For each observed H_2 emission line we compute the column density $N(v, J)$ in the excited state required to reproduce the observed surface brightness, for an assumed foreground extinction $A_K = 0.5\text{mag}$.

A detailed discussion of our modelling of NGC 2023 will be reported elsewhere, but here we show one example of a model developed to reproduce the observations of the southern emission bar. We assume the incident radiation field to be enhanced by a factor $\chi \approx 5000$ relative to the Habing (1968) flux, and a gas density $n_{\text{H}} = 5 \times 10^4 \text{cm}^{-3}$. The PDR is assumed to be plane-parallel, inclined relative to the line of sight with $\cos \theta = 0.2$, where θ is the angle between the normal to the PDR (= the direction from the PDR to the illuminating star) and the direction to the Earth.

In Figures 2–4 we show $N(v, J)/g_J$ for the model together with the observed level populations, versus the energy $E(v, J)$ of the excited state. Open symbols are model results; filled symbols are observations. The model is seen to be in quite good agreement with the populations of the vibrationally-excited levels all the way up to $v = 12$! The generally excellent agreement between model and observations indicates that the description of the ultraviolet pumping process is basically sound. The fact that for a given vibrational level the rotational level populations appear to be in good agreement with observations indicates that the model has approximately the correct temperature and density. Only for a few weak lines are the reported fluxes very different from the model predictions: 12-6 Q(5) $\lambda = 0.8225\mu\text{m}$, where the reported flux is a factor of 20 stronger than expected, and 9-4 S(11) $\lambda = 0.7663\mu\text{m}$, where the observed flux is a factor ~ 7 stronger than expected. With so many other lines in good agreement, perhaps these lines have been misidentified. Note, however, that these are the only two lines from levels with $E(v, J)/k > 48 \times 10^3\text{K}$, so perhaps there are processes populating these very high energy levels which have not been included in the model (see Bertoldi et al. 2000b).

Figure 5 shows the $v = 0$ level populations for our model, together with the level populations inferred from the ISO observations toward NGC 2023 (Bertoldi et al. 2000a), except that the surface brightnesses measured by the relatively large ISO beam have been arbitrarily increased by a factor 1.8 – the reasoning here is that the bright southern bar represents a region with unusually high limb-brightening, probably about a factor of 2 higher than the average over the ISO beam. With this adjustment, we obtain quite good agreement for most of the rotational levels; the largest discrepancy is for $J = 3$, where the model surface brightness is about twice the observed value. Note that the observed

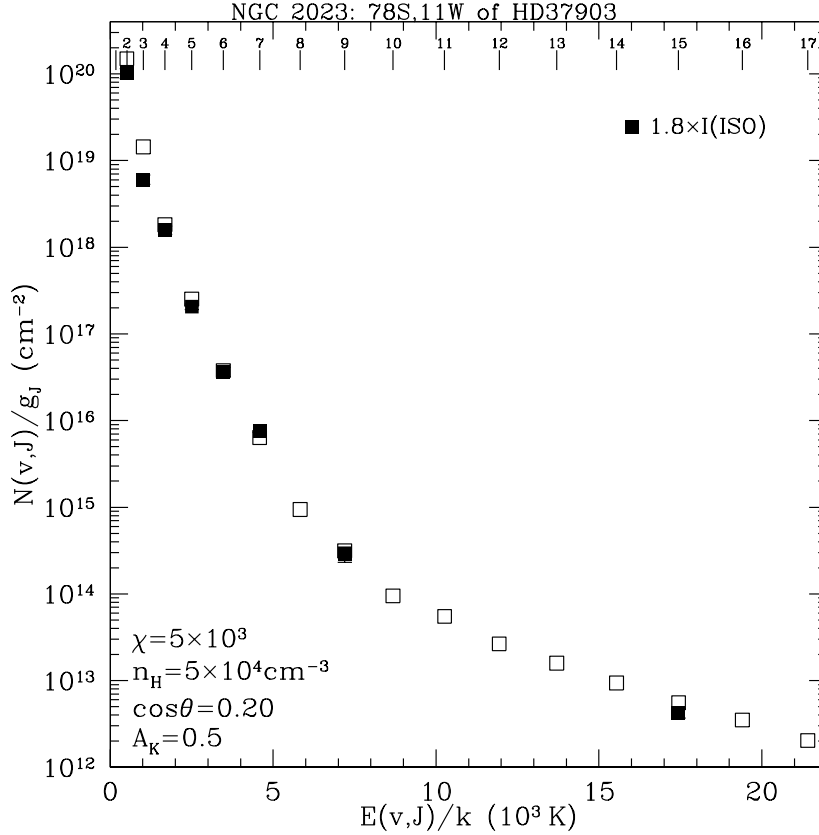


FIGURE 5. Level populations for rotationally-excited levels of the ground vibrational state in NGC 2023. Beam-averaged column densities observed by ISO have been multiplied by 1.8 to allow for likely enhancement of the surface brightness on the southern bar.

emission from the $J = 15$ level is in excellent agreement with the model! The level populations obviously depart strongly from a single-temperature fit; this is mainly due to the range of gas temperatures present (see Figure 6) and the excitation of newly-formed H_2 leaving grain surfaces.

The model is shown in Figure 6. Photoelectric emission from dust grains dominates the heating over much of the PDR, but for $10^{19} \lesssim N_{\text{H}} \lesssim 10^{21} \text{ cm}^{-2}$ the dominant heat source is collisional deexcitation of H_2 which has been vibrationally excited by UV pumping. The combination of photoelectric heating and heating by deexcitation of H_2 manages to maintain a gas temperature of $\sim 10^3 \text{ K}$ over a substantial zone, with the gas temperature still as high as $\sim 700 \text{ K}$ when the H_2 fraction has risen to 10%.

The model assumes gas phase abundances $\text{C}/\text{H} = 1.4 \times 10^{-4}$ (1/3 solar), $\text{O}/\text{H} = 3.2 \times 10^{-4}$ (1/2 solar), $\text{Si}/\text{H} = 9.0 \times 10^{-7}$ (1/40 solar), $\text{Fe}/\text{H} = 1.3 \times 10^{-7}$ (1/250 solar). Predicted fine structure line intensities for the bright southern bar (for limb-brightening $1/\cos \theta = 5$) are given in Table 1. Most of the lines are not yet observed, but the intensity measured by ISO for $[\text{Si II}] 34.8 \mu\text{m}$ is only 1/25 of the model prediction! Part of the discrepancy can be attributed to beam dilution: the ISO beam is 660 arcsec^2 , whereas the bright bar is only $\sim 50 \text{ arcsec}^2$. However, there presumably is $[\text{Si II}]$ emission away from the bar, so it appears likely that the Si is depleted by ~ 400 relative to solar. It is interesting to compare this with the S140 PDR, where the inferred Si abundance was 1/40 solar

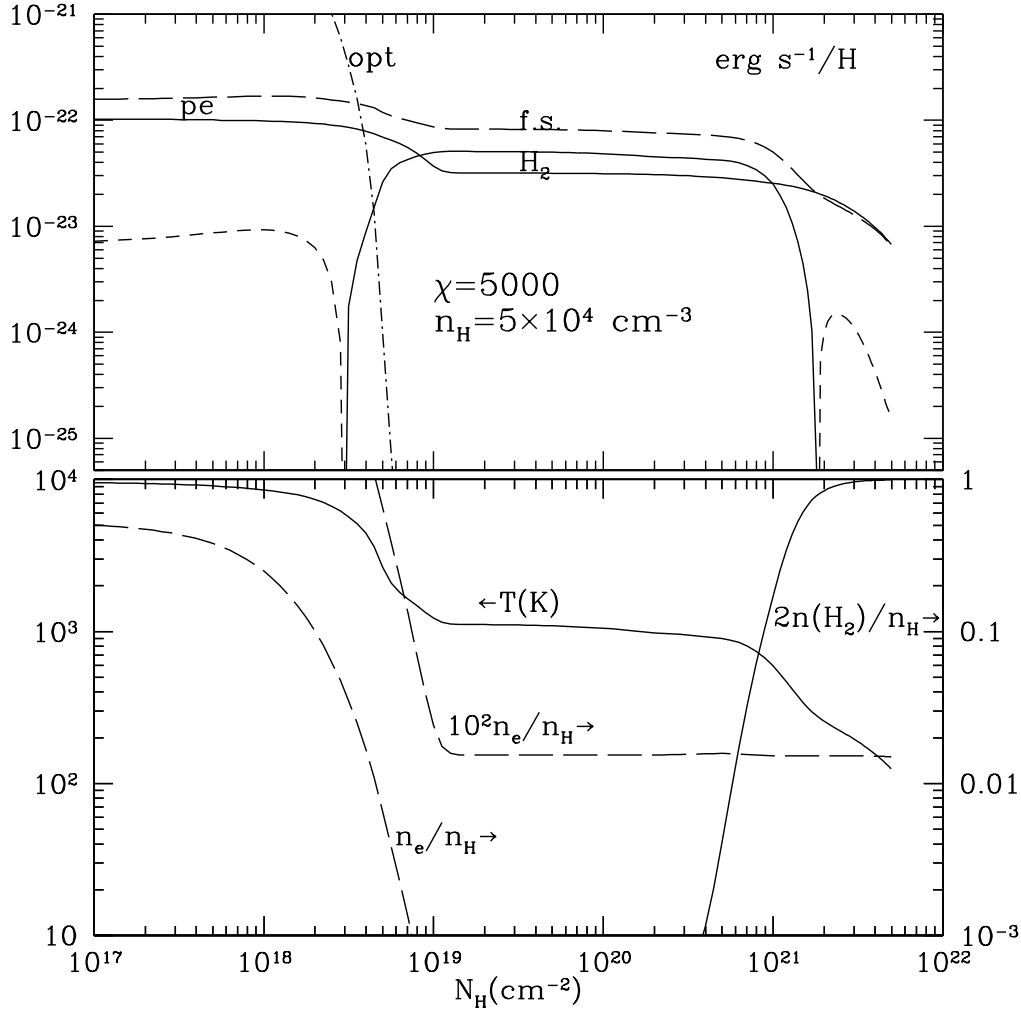


FIGURE 6. Lower panel: temperature T , ionization fraction n_e/n_H , and H_2 fraction as function of column density N_H measured from the ionization front. Upper panel: Heating or cooling contributions due to photoelectric emission from dust (p.e.), fine structure emission (f.s.), optical line emission (opt), and collisional excitation/deexcitation of H_2 (H_2). Solid lines indicate heating; broken lines indicate cooling. H_2 heats the gas over the region $5000 \gtrsim T \gtrsim 300K$.

(Timmermann et al. 1996). Walmsley et al. (1999) have recently discussed the puzzling variations in Si abundance observed in PDRs.

5. Discussion

There are a number of areas for improvement in our modelling of PDRs:

- We need accurate cross sections for collisional excitation and deexcitation of H_2 .
- We need to understand the details of the H_2 formation process in PDRs – the overall rate and the (v, J) distribution of newly-formed H_2 .
- The rate of photoelectric heating by dust is critical, particularly since drift of the dust grains can alter the dust/gas ratio in the PDR (Weingartner & Draine 1999, 2000b).
- Finally, we need more accurate spectrophotometry, with refined angular reso-

line	predicted	observed	
[SiII]34.81 μ m	1.5×10^{-3}	5.7×10^{-5}	erg cm ⁻² s ⁻¹ sr ⁻¹
[FeII]25.99 μ m	1.8×10^{-4}	-	
[OI]63.18 μ m	4.5×10^{-2}	-	
[OI]145.5 μ m	2.9×10^{-3}	-	
[CII]157.7 μ m	4.6×10^{-3}	-	

TABLE 1. NGC 2023 Fine Structure Line Emission

lution, to allow us to understand the geometry of the filaments and sheets which are apparent in high-resolution images of NGC 2023 and other PDRs.

This research was supported in part by NSF grant AST96-19429.

REFERENCES

- ABGRALL, H., & ROUEFF, E. 1989, *A&A Suppl.*, **79**, 313-328.
 ABGRALL, H. ET AL. 1993a, *A&A Suppl.*, **101**, 273-321.
 ABGRALL, H. ET AL. 1993b, *A&A Suppl.*, **101**, 323-362.
 BERTOLDI, F., ET AL. 2000a, in preparation
 BERTOLDI, F., & DRAINE, B.T. 1996, *ApJ*, **458**, 222-232.
 BERTOLDI, F., ET AL. 2000b, in *Astrochemistry*, IAU Symposium 197, ed. Y.C. Minh & E.F. van Dishoeck (San Francisco: Astr. Soc. Pac.) in press.
 BLACK, J.H., & VAN DISHOECK, E.F. 1987, *ApJ*, **322**, 412-449.
 BURTON, M.G., ET AL. 1998, *PASA*, **15**, 194-201
 DRAINE, B.T., & BERTOLDI, F. 1996, *ApJ*, **468**, 269-289.
 FIELD ET AL. 1998, *A&A*, **333**, 280-286
 HABING, H.J. 1968, *Bull. Astr. Soc. Neth.*, **19**, 421-431.
 MCCARTNEY, ET AL. 1999, *MNRAS*, **307**, 315-327
 ROUAN ET AL. 1997, *MNRAS*, **284**, 395-400
 STEPHENS, T.L., & DALGARNO, A. 1973, *ApJ*, **186**, 165-167
 TIMMERMANN, R., ET AL. 1996, *Astr.Ap.*, **315**, L281-284.
 WALMSLEY, C.M., PINEAU DES FORETS, G., & FLOWER, D.R. 1999, *A&A*, **342**, 542-550.
 WEINGARTNER, J.C., & DRAINE, B.T. 1999, in *The Universe as seen by ISO*, ed. P. Cox & M.F. Kessler, (Nordwijk: ESA), 783-786.
 WEINGARTNER, J.C., & DRAINE, B.T. 2000a, *ApJ*, submitted
 WEINGARTNER, J.C., & DRAINE, B.T. 2000b, in preparation